

Article

Chemical Behaviour of Copper in the Application of Unconstrained Cr-Ni-Al-Cu Metal Powders in Submerged Arc Welding: Gas Phase Thermodynamics and 3D Slag SEM Evidence

Theresa Coetsee *  and Frederik De Bruin

Department of Materials Science and Metallurgical Engineering, University of Pretoria, Pretoria 0002, South Africa

* Correspondence: theresa.coetsee@up.ac.za

Abstract: Unconstrained metal powders of Cu, Cr, Ni and Al were applied to submerged arc welding (SAW) to clarify the chemical behaviour of copper in this modified SAW process. Aluminium metal is avoided in SAW because it is easily oxidised. Excessive aluminium oxides in the form of slag or inclusions in the weld metal will lead to poor weld metal materials properties. Aluminium is an effective deoxidiser and can be used to prevent Cr and Ni loss to the slag by preventing oxidation of these metals. The results show that carbon steel was alloyed to 5.3% Cr, 5.3% Ni, 3.6% Al and 5.2% Cu at 80% Cr yield, 81% Ni yield, 54% Al yield and 79% Cu yield. BSE (backscattered electron) images of the three-dimensional (3D) post-weld slag sample show 3D structures within the slag dome. The 3D structures contain features of vapour formation and recondensation. In addition, nano-strands appear in the 3D structures and confirm the vaporisation and recondensation of fluorides. The chemical behaviour of copper metal powder added in SAW is to vaporise as metallic copper and incorporate in the Al-Si-Mg-Ca-Mn-Fe-Cu-Na-Cr-Ni fluoride. Copper, in combination with aluminium, has a stabiliser effect in SAW due to its formation of an initial alloy melt of low liquidus temperature, thus decreasing the temperature required to melt high-melting-point metals such as Cr into the weld pool. Although Al and Cu have similar vapour pressures at specific temperatures, it appears that Cu does not substitute for Al in the gas phase. Gas-slag-alloy thermochemical equilibrium calculations confirm the partial oxygen pressure lowering effect of aluminium and the vaporisation of copper as metallic copper with very little copper-fluoride species expected to form. The quantity of metallic copper vaporisation calculated in the gas-slag-alloy thermochemical equilibrium is much higher than the vaporisation quantity measured in welding. This may be due to recondensation of vaporised copper which is not accounted for in the equilibrium calculation at the set arc cavity temperature, as well as the effect of surface-active elements such as sulphur and oxygen in limiting the vaporisation reaction of copper.

Keywords: pyrometallurgy; powder; nickel; chromium; copper; partial oxygen pressure; aluminium deoxidiser; welding



Citation: Coetsee, T.; De Bruin, F. Chemical Behaviour of Copper in the Application of Unconstrained Cr-Ni-Al-Cu Metal Powders in Submerged Arc Welding: Gas Phase Thermodynamics and 3D Slag SEM Evidence. *Processes* **2023**, *11*, 351. <https://doi.org/10.3390/pr11020351>

Academic Editors: Blaž Likozar and Alexander Novikov

Received: 14 December 2022

Revised: 3 January 2023

Accepted: 19 January 2023

Published: 21 January 2023



Copyright: © 2023 by the authors. Licensee MDPI, Basel, Switzerland. This article is an open access article distributed under the terms and conditions of the Creative Commons Attribution (CC BY) license (<https://creativecommons.org/licenses/by/4.0/>).

1. Introduction

Submerged arc welding (SAW) is the preferred welding method to join thick steel plates at high productivity rates [1]. SAW can also be used as a high-productivity method for cladding and hard facing of inferior and cheaper substrate materials [2]. The fundamental aspects of the SAW process remain the same despite these different SAW process applications.

The flux applied in SAW serves a variety of functions which sets the process metallurgy of the SAW process via pyrometallurgical reactions in the arc cavity, weld pool and slag layer. One important function of the flux is to control the weld metal total oxygen (ppm O). High-impact toughness is ensured if the weld metal total oxygen content is controlled at 200–500 ppm O [3]. A much higher quantity of oxygen is initially present in the weld pool after

its transfer from the molten weld wire droplets in the arc cavity, namely 2000–3000 ppm O [4,5]. Therefore, this high initial quantity of 2000–3000 ppm O must be decreased to 200–500 ppm to attain weld metal of acceptable impact toughness. The high initial quantity of 2000–3000 ppm O is sourced solely from the decomposition of flux oxides at the high temperatures (2000 °C to 2500 °C) in the arc cavity [6]. Because such high temperatures prevail in the arc cavity, 2000 °C to 2500 °C, the oxide arc plasma stability should correspond to the oxide thermodynamic stability [7,8]. However, it was determined experimentally that there is a unique arc plasma stability order for the oxides that are typically applied in SAW fluxes. In these welding tests, SAW under argon gas was conducted with the application of a different oxide–CaF₂ flux mixture in each test, and then the total ppm O was analysed in the weld metal [9]. A higher weld metal total ppm O from these test welds confirmed that the particular metal oxide in the oxide–CaF₂ flux is less stable in the arc, because it dissociates in the arc plasma to release more oxygen. This work concluded that the oxide arc plasma stability order follows the sequence of CaO, K₂O, Na₂O, TiO₂, Al₂O₃, MgO, SiO₂ and MnO as the least stable oxide [9]. Increased quantities of CaF₂ in the flux dilute the low-stability oxides to lower the weld metal total ppm O. An empirically determined trend line of the basicity index of the flux (BI) vs. weld metal total ppm O is typically used in the welding consumables industry [10]. The BI is expressed in Equation (1) in mass% quantities. Based on this trend line, at flux BI values in excess of 1.5 the weld metal total ppm O is constant at 250 ppm O [10]. The weld metal hydrogen content is also minimised at these high flux basicities [7,10].

$$BI = \frac{\%CaF_2 + \%CaO + \%MgO + \%BaO + \%SrO + \%Na_2O + \%K_2O + \%Li_2O + 0.5(\%MnO + \%FeO)}{\%SiO_2 + 0.5(\%Al_2O_3 + \%TiO_2 + \%ZrO_2)} \quad (1)$$

Flux chemistry is also an important input to maintain arc stability and to attain desired arc plasma behaviours. For example, alkali metal oxides (K₂O and Na₂O) may be added to stabilise the arc [11]. In recent studies, high-speed imaging and spectroscopy were used to elucidate arc cavity phenomena in SAW [12]. The gas phase analyses showed qualitatively that different elements dominate in the gas phase depending on the particular flux formulation used [1,12]. These works confirm that arc physical phenomena are heavily influenced by flux chemistry. Increased CaF₂ additions to the flux decrease the arc length by decreasing plasma conductivity via changes in the proportions of fluorine to oxygen in the gas phase [13]. In addition, the flux CaF₂ content influences the slag electrical conductivity, and excessive CaF₂ additions may cause current loss to the slag shell [1]. Therefore, the flux chemical formulation not only drives the process metallurgy of SAW, but also determines the arc plasma phenomena, which are important in arc energy generation and metal transfer to the weld pool [1,12,13].

Fluxes are also used to add elements from the oxides in the flux to the weld pool. Therefore, the flux composition is specified to achieve a targeted quantity of element transfer from the flux to the weld pool during the welding process. [14–17]. Consequently, changes made to a flux chemistry formulation, as well as the weld wire and base plate chemistries, must be re-evaluated to measure the end-point weld metal composition attained from the SAW process.

Chromium has a high affinity for oxygen and is therefore not easily transferred across the arc [18]. Chromium oxide vaporisation losses have been reported from chromium oxide containing flux [19]. Chromium oxide is considered to react in SAW in the same way as Al₂O₃ in Equation (1), implying that it is an oxygen supplier compound in the flux [19]. Because of the above chemical complications, chromium is added to the weld pool via weld wire, often with nickel as stainless-steel wire [18]. A limited number of weld wire formulations are available on the market because of the time and expense demands of manufacturing. The result is that the available weld wire formulations cannot closely match all the different alloy compositions that may be required. Alloying of the weld metal via metal powders in combination with a solid arching wire can result in better matching of the weld metal to the base plate material [20]. The application of metal powders in SAW was

demonstrated in cladding with chromium-nickel pre-alloyed iron-based powders [20]. The overall deposition productivity is also improved when metal powder is used in addition to the one arching wire. From the reported application examples of pre-alloyed powders in SAW, the Ni and Cr yield values were as follows: nickel yield values ranged from 57% to 78%, and chromium yields varied from 56% to 76%. The pre-alloyed iron-based powders contained 27–29% Cr, 5–8% Ni and 2–4% Mo [20]. However, the manufacturing of pre-alloyed powder is also time consuming, and as is the case with solid weld wires, the pre-alloyed powders cannot closely match all desired alloy compositions. A better option in terms of lowering cost and manufacturing time is to use unconstrained metal powders in SAW to alloy the weld metal. Unconstrained metal powders refer to non-alloyed metal powders which are not constrained in tubular wire, such as flux cored and metal cored wire. In our previous studies, we illustrated the application of unconstrained metal powders of pure Al, Cr and Ni in SAW. The yield numbers from the metal powders to the weld pool was 67%, 89% and 91%, and the weld metal total oxygen content was controlled to 162 ppm O [21].

Aluminium metal addition in SAW is avoided because Al is easily oxidised and can then form excessive quantities of inclusions and/or slag to the detriment of the weld metal materials properties. In this work, we use our novel application of aluminium metal powder in SAW which ensures the modification of flux oxygen behaviour to control the weld metal total ppm O within acceptable quantities, similar to our previous works [21–29]. Because the alloying element yield is dependent on the flux-induced partial oxygen pressure, the element yield can be improved by deoxidiser application, as illustrated in our previous studies [21–29]. New classes of steels are formulated with aluminium as a necessary building block element required in large quantities in the steel formulation, namely low-density/high-entropy steels and low-density stainless steels [30,31]. Thus, the combination of alloying elements with aluminium in steel formulations will become increasingly important and needs to be applied in SAW to ensure that the SAW process can also be applied to these steel grades.

Copper has traditionally been avoided in steel formulations because it creates the well-known phenomenon of “hot shortness” during hot rolling operations. However, once this formation mechanism was better understood and negated, the benefit of copper as an alloying element in steel was realised. More recently, copper has been added to carbon steels and stainless steels to enhance mechanical and corrosion properties [32]. For example, 4% copper added to chrome-manganese stainless steels improves corrosion resistance, whilst maintaining good weldability [32]. In terms of welding consumables, the use of copper as an alloying element presents some challenges. For example, alloying of the weld wire with copper forms a weld wire that work hardens. Such a copper-containing alloy is not easily formed into wire product, and it is also not easily passed through the roller guide system of the SAW equipment [33]. These difficulties may be avoided by adding copper to the SAW weld pool as metal powder. In our previous studies, we showed that copper, in combination with aluminium, has a stabiliser effect in SAW due to its decreasing of the temperature required to melt high-melting-point metals such as Ti or Cr into the weld pool, by forming an initial alloy melt of low liquidus temperature [26,27].

The objective of this study is to reveal the chemical behaviour of Cu in the application of unconstrained metal powders of Al, Cr, Ni and Cu in SAW, specifically the gas phase reactions of copper. We present three-dimensional (3D) post-weld slag sample phase chemistry analyses by SEM (scanning electron microscopy) to investigate the speciation and element distribution of Cu in the slag. Thermodynamic modelling is used in the form of gas-slag-metal powder reaction equilibrium calculations to deduce the chemical behaviour of Cu from the interaction between welding flux and Al, Cr, Ni and Cu metal powders in SAW.

2. Materials and Methods

2.1. Welding Tests

Welding tests were performed as described previously [34]. The photographs in Figure 1 shows the weld metal cross-sections of BC and MP10 weld metals.

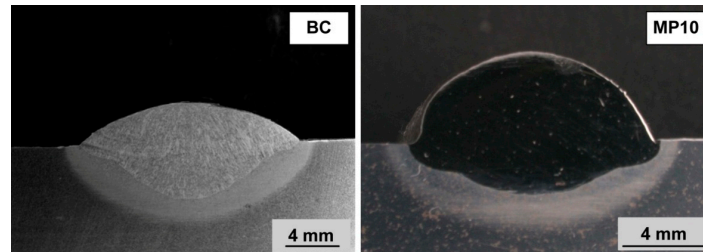


Figure 1. Photograph of BC and MP10 weld metal cross-sections.

The input materials (base plate, weld wire and flux) analysis method details were previously described in our prior publication [23]. The base plate is low carbon steel of 1.340% Mn and 0.155% Si as the main alloying elements [23]. The weld wire has 0.990% Mn and 0.137% Si [23].

2.2. Thermochemical Calculations for Gas Phase Reactions

The thermochemical software, Factsage 7.3, was used to calculate the three-phase gas-slag-metal equilibrium from gas, slag and metal powder inputs as described previously [22]. This gas-slag-metal equilibrium model is similar to the simulation model described in detail elsewhere and was successfully applied to calculate the carbon steel weld metal total ppm O in SAW for different flux formulations [35]. Because it is clear from changes in the weld metal analysis that some of the added Al reacted with MnO and SiO₂ in the slag, the proportion of the feed aluminium quantity that possibly participated in the gas reactions was varied to gauge the role of different quantities of Al in the gas phase reactions. The thermodynamically predicted gas phase species from these calculations showed the likely gas phase reaction changes induced by the added metal powders of aluminium, chromium, nickel and copper. The databases that were selected in the Equilib module in FactSage 7.3 were the FToxid, FSstel and FactPS databases. In addition, plasma species were included as part of the gas phase [36]. The calculation results are discussed in Section 4.1.

3. Results

3.1. Weld Metal Chemical Analyses

Table 1 displays the bulk weld metal chemical analyses for the BC weld metal made without metal powder additions and the MP10 weld metal made with added Al, Cr, Ni and Cu powders. The methods used to cut samples from the weld metal and the chemical analyses techniques used were previously described in detail [28]. In addition to the bulk weld metal analyses in Table 1, EDS analyses of marked areas as displayed in Figure 2 were made for comparison purposes. The position of the micrograph in Figure 2 is at the geometric centre of the MP10 weld metal cross-section. The EDS analyses of the areas marked in Figure 2, as displayed in Table 2, are in agreement with alloying of the weld metal with Al, Cr, Ni and Cu. SEM equipment used for the EDS analyses were described previously [28].

Table 1. Bulk chemical analyses of weld metals (mass%).

	%C	%Si	%Mn	%O	%Al	%P	%S	%Ni	%Cr	%Cu	%Fe
Base Case	0.110	0.260	1.300	0.0499	0.032	0.022	0.011	0.005	0.110	0.110	98.03
MP10	0.105	0.763	1.437	0.0184	3.597	0.024	0.009	5.277	5.290	5.153	78.24

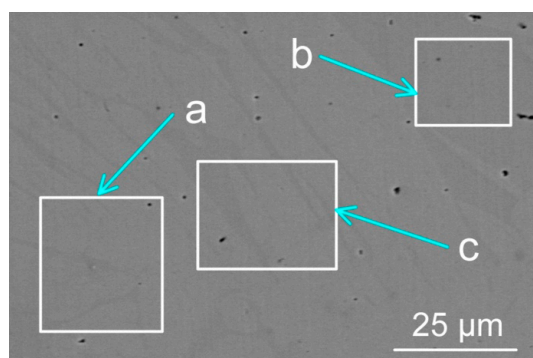


Figure 2. SEM micrograph of weld metal with areas marked a, b and c (see Table 2 below, indicating the analyses per marked phase areas: a, b and c) ($\times 2600$).

Table 2. SEM-EDS analyses of marked areas in the MP10 weld metal as indicated in Figure 2 (mass%).

	%Si	%Mn	%Al	%Ni	%Cr	%Cu	%Fe
a	0.84	1.44	3.21	4.83	4.99	4.52	80.2
b	0.82	1.50	3.30	4.89	4.96	4.68	79.8
c	0.84	1.45	3.29	5.02	4.96	4.78	79.7

Comparison of the analyses data for the BC and MP10 weld metals in Table 1 confirm increased silicon and manganese contents in the MP10 weld metal. The explanation for this change in weld metal chemistry is that MnO and SiO₂ in the slag were reduced by Al according to Equations (2) and (3). This effect was also identified in our previously reported work on aluminium-assisted alloying via different metal powders in SAW [21–29]. Therefore, the aluminothermic reduction reactions in Equations (2) and (3) also occurred in the MP10 weld run. Reactions in Equations (4) and (5), the aluminothermic reduction of FeO and CrO may also occur, even though the reaction extent is not as clear as that of the reactions in Equations (2) and (3). Our previous similar works on SAW with different metal powder combinations with aluminium showed that FeO formed due to oxidation of weld pool iron by the excess oxygen transferred from the arc cavity [37,38]. The aluminothermic reduction of FeO via Reaction (4) indicates control of the oxygen potential at the weld pool–slag interface [21–29]. Similarly, chromium oxide can be reduced by aluminium via Reaction (5) [24].



(): liquid.

The differences in weld metal total ppm O in Table 1 of 499 ppm O in the BC weld metal vs. the significantly lower value of 184 ppm O in the MP10 weld metal is due to the deoxidising effect of the added metal powders, in particular Al as a deoxidiser element.

3.2. Mass Balance for Yield from Metal Powders

A mass balance was done to quantify the yield of Al, Cr, Ni and Cu from the added metal powders to the weld metal. The details of the mass balance measurements and calculations were described previously [21,25–29]. The %yield of each alloying element from the individual metal powder to the weld metal can be calculated once the gram mass of each alloying element (Al, Cr, Ni and Cu) is known from the mass balance calculations as displayed in Table 3. The %yield is calculated as a percentage of the 7 g of Al or Cr or Ni

or Cu added to the weld run. The %yield numbers from the mass balance calculations in Table 3 show 54% Al yield, 80% Cr yield, 81% Ni yield and 79% Cu yield from each pure metal powder to the weld metal.

Table 3. Mass balance numbers and percentage yield calculation results for Al, Ni, Cr and Cu.

	Al (g)	Cr (g)	Ni (g)	Cu (g)	Powder (g)	Wire (g)	Base Plate (g)	Weld Metal (g)	%DR _(wire + MP)	%Al Yield	%Cr Yield	%Ni Yield	%Cu Yield
MP10	3.8	5.7	5.6	5.5	20.7	49.3	37.0	107.0	65	54	80	81	79

3.3. Quantification of the Exothermic Reactions with Aluminium

The alumina formed as a product in Reactions (2) and (3) was shown to be easily absorbed into the molten flux because the reactions occurred at the molten flux–weld pool interface [21–29]. The exothermic reaction heat contribution from Reactions (2) and (3) was quantified in the same way as reported in our previous works [25–29]. The results are summarised in Table 4. Even though these quantities are relatively small, the exothermic heat released from these reactions is sufficiently large to significantly increase the weld metal temperature by 70 °C.

Table 4. Exothermic heat added to the weld pool from reactions (2) and (3).

	SiO ₂ (g)	MnO (g)	Al (g)	Reaction (2) (kJ)	Reaction (3) (kJ)	Reactions (2) & (3) (kJ)	Weld Metal ΔT (°C)
MP10	1.41	0.37	0.94	−2.57	−0.87	−3.44	70

The time available for oxide inclusions to float from the weld pool to the molten slag–weld pool interface is set by the weld pool solidification time [39]. Once the oxide inclusions reach the slag–weld pool interface, they may be absorbed into the slag and thus be removed from the weld pool [39]. The weld pool cooling time is set by the difference between the weld pool liquidus and solidus temperature. It is expected that the weld pool cooling time will change with changed weld pool chemistry. To check for this effect, the cooling curves for the BC and MP10 weld metal compositions are shown in Figure 3. From Figure 3 it is seen that the MP10 weld metal solidus temperature is much lower than the BC weld metal solidus temperature, and the liquidus temperature is lowered by 50 °C due to added alloying elements in the MP10 weld metal. It is expected that the MP10 weld metal will take a longer period of time to solidify, providing more time for oxide inclusions to float to the weld pool–slag interface and absorb into the slag layer. This difference in solidification time is a contributing factor in changing the weld metal total ppm O from the higher value in the BC weld metal to the lower value in the MP10 weld metal; see Table 1.

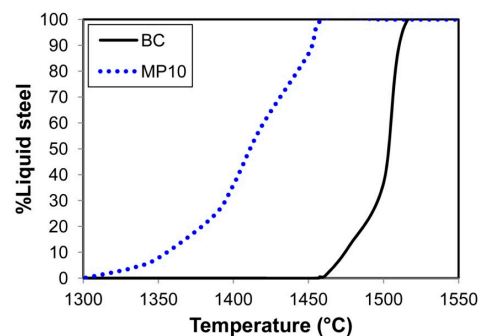


Figure 3. Solidification curves for MP10 and BC weld metal.

3.4. Chromium, Nickel and Copper Speciation and Distribution in the Slag

In our previous works, SEM (scanning electron microscope) and EDX (energy dispersive X-ray) analyses were applied to study the speciation and distribution of the elements in post-weld slags [22,38]. This work clearly showed the presence of 3D structures which formed from vaporisation and recondensation of oxy-fluorides. The same type of analyses on 3D post-weld slag from the MP10 weld test were used here to confirm that the same oxy-fluoride behaviour exists once Cu is added as an alloying element.

Figure 4a displays a low magnification BSE (backscattered electron image) image of the 3D slag sample with the arrow marking one of the 3D structures contained within the slag dome. This 3D structure is shown enlarged in Figure 4b, and the EDX analyses for this structure are shown in Figure 4c. The average analysis of the field of view in Figure 4b is shown in Table 5, indicating that it consists of Si-Al-Ca-Mg-Na-K-Fe-Mn-Ni-Cr-Cu oxy-fluoride. In comparison, the element distribution in the EDX analyses maps displayed in Figure 4c indicates that the 3D structure contains Si-Na-Fe-Mn-Ni-Cr-Cu oxyfluoride, and the matrix slag contains Al-Mg-Ca-Si-Na oxy-fluoride. The enlarged part in the blocked area of Figure 4b is shown in Figure 4d. The average analysis of this field of view is shown in Table 6, indicating the absence of oxygen in the fluoride which contains Al-Si-Mg-Ca-Mn-Fe-Cu-Na-Cr-Ni. The presence of nano-strands is seen in Figure 4d. This appearance of the nano-strands is similar to that of the nano-strands identified in our previous 3D post-weld slag samples [38]. Therefore, the presence of copper in these structures confirms the vaporisation of copper which could only be sourced in significant quantities from the added copper metal powder, similar to the vaporisation of added Al, Cr and Ni metal powders shown previously [21,22,38].

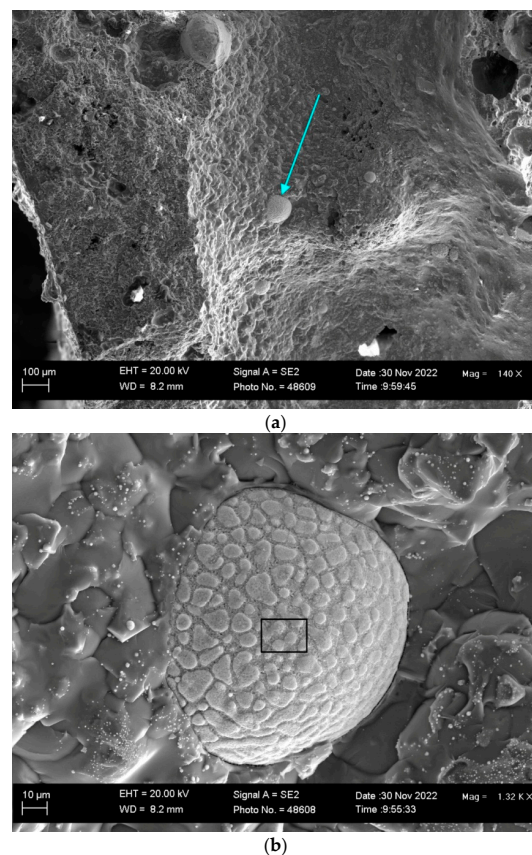


Figure 4. Cont.

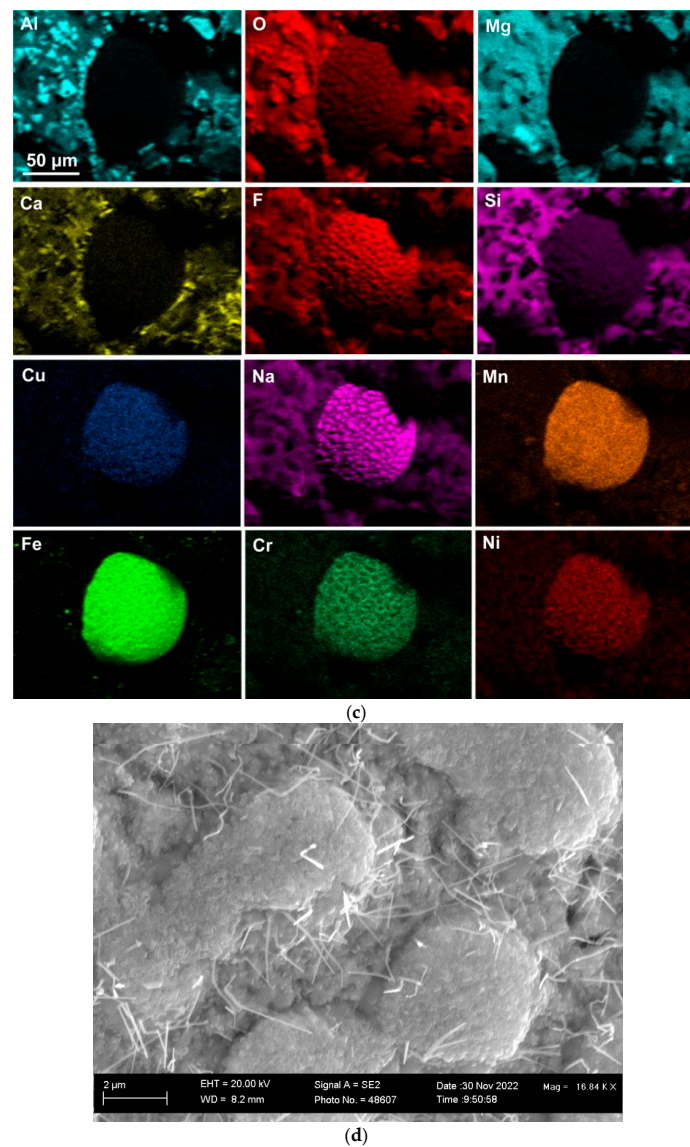


Figure 4. (a) BSE image at 140× magnification showing a slag dome in the MP10 post-weld slag; (b) BSE image at 1320× magnification of the 3D structure marked with arrow in (a); and (c) EDX maps of 3D slag structures in (b); (d) BSE image at 16,840× of 3D structure in blocked area in (b).

Table 5. EDS analyses of the field of view in Figure 4b.

	%F	%O	%Al	%Si	%Mg	%Ca	%Mn	%Fe	%Cu	%Na	%K	%Cr	%Ni
Slag	17.6	21.4	10.4	8.0	12.2	2.9	6.2	14.5	0.4	4.8	0.4	0.9	0.3

Table 6. EDS analyses of the field of view in Figure 4d.

	%F	%O	%Al	%Si	%Mg	%Ca	%Mn	%Fe	%Cu	%Na	%K	%Cr	%Ni
Slag	26.5	0.0	0.5	3.3	0.9	0.1	12.9	40.1	1.3	11.2	0.0	2.4	0.8

4. Discussion

In this study, as in our previous studies, aluminium powder was applied in SAW to control the weld metal total ppm O [21–29]. The partial oxygen pressure at the molten flux–weld pool interface is lowered by the deoxidiser effect of Al when added to the SAW process [29–36]. Even without the addition of Al, but in the presence of Al_2O_3 in the flux,

aluminium is also present in the arc cavity as Al vapour, and this Al can therefore also lower the oxygen partial pressure in the arc cavity [21,22,29,40]. Addition of copper metal powder with chromium, nickel and aluminium metal powders in the SAW process may modify the behaviour of aluminium in the arc cavity because both metals have similar high vapour pressures. In the following section, thermochemical calculations of the gas-slag-metal powder equilibrium are applied to investigate the likely gas phase reaction changes from adding the combination of copper, chromium, nickel and aluminium powders in the SAW process.

4.1. Thermochemical Equilibrium Calculations

The vaporisation curves of the major metallic elements present in the welding process are displayed in Figure 5. The lines in Figure 5 show that the order of ease of vaporisation of the pure elements ranges from highest to lowest: Mn, Al, Cu, Cr, Fe, Ni and, lastly, Si. Figure 5 confirms that aluminium and copper are expected to be vaporised to an equal extent at the high temperatures prevailing in the arc cavity, 2000 to 2500 °C [7,8].

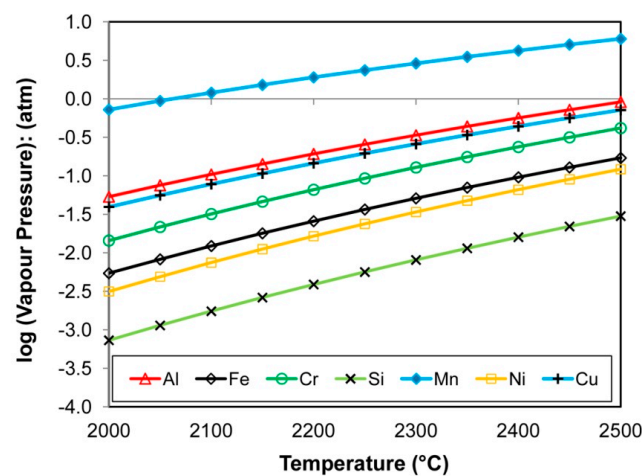


Figure 5. Vapour pressure of pure metals Mn, Al, Cr, Fe, Ni, Si, Cu vs. temperature.

In our previous studies, we showed that copper, in combination with aluminium, has a stabiliser effect in SAW due to its formation of an initial melt of low liquidus temperature, thus decreasing the temperature required to melt high-melting-point metals such as Ti and Cr into the weld pool [25,26]. The same effect is illustrated in the liquidus projection diagram in Figure 6. The proportion of Cr to Ni is the same as in the added metal powders and in the weld metal analysis in Table 1. The composition point in Figure 6 (filled circle) is the equivalent composition point for the Cr-Ni-Cu-Al ratios in the MP10 weld metal composition in Table 1. The information in Figure 6 indicates that this mixture of metal powders was completely liquid at 1300 °C, which is much lower than the liquidus temperature of the base case weld metal as displayed in Figure 3, at about 1516 °C. However, this stabiliser effect of copper in the alloy and steel phases does not take the gas phase reaction behaviour of copper into consideration. Although copper is less easily oxidised to its oxide compared to the easily oxidised elements such as Cr and Al, the interaction of copper with other elements in the arc cavity should be investigated.

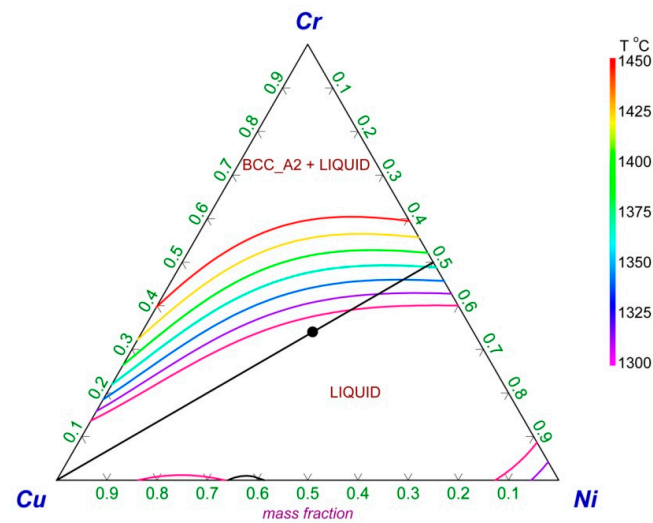
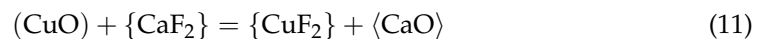
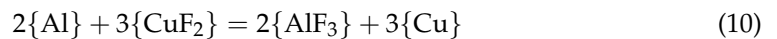
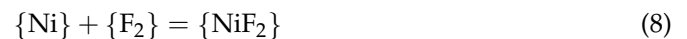


Figure 6. Cr-Cu-Ni-19% Al liquidus projection diagram calculated in FactSage 7.3 [36].

The standard Gibbs free energy lines in Figure 7 confirm that the reaction of copper vapour with fluorine gas, to form $\text{CuF}_2(\text{g})$ according to Reaction (6), is the least likely reaction amongst the metals under consideration here; see Reactions (6)–(9). The lines in Figure 7 were calculated by using the following input values: 1 atm for each gas, namely metal vapour, $\text{F}_2(\text{g})$ and the product metal fluoride gas. As discussed in our previous similar analyses on the interaction of Al, Cr, Ni and Co metal vapour and their gaseous fluorides, it is implied from the data in Figure 7 that Reaction (10) will be able to transform any $\text{CuF}_2(\text{g})$ to $\text{Cu}(\text{g})$ via reaction with Al. Since copper is not easily oxidised, Reaction (11) is not expected to play a role in the chemical behaviour of copper in SAW.



(): liquid; { }: gas; < >: solid.

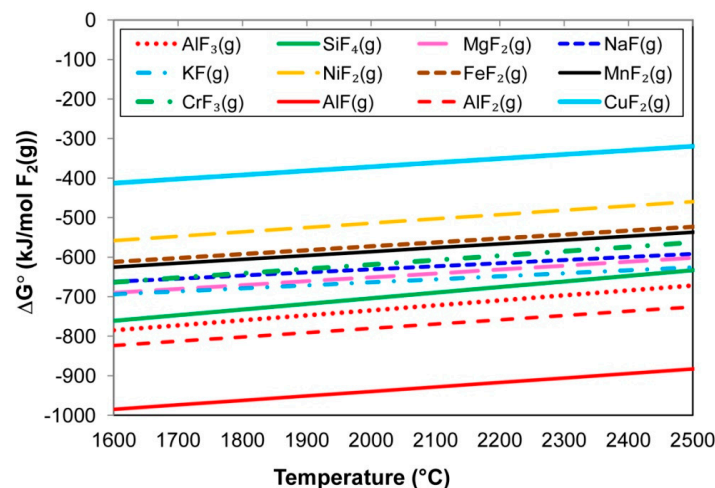


Figure 7. Standard Gibbs free energy values of reactions similar to Equations (6)–(9).

The above reaction and vaporisation reactions were investigated for the individual metals, and this simplified approach did not simulate the interaction between different chemical compounds, especially in the gas phase. Therefore, more realistic thermochemical calculations were performed to investigate the probability of species formation, especially in the gas phase as described in Section 2.2.

The chromium, nickel and copper metal powder input masses to the weld, at 7 g each, were specified as inputs to the calculation. The proportion of the Al input mass in the calculation was varied between zero, 50% and 100% of the maximum of 6.1 g Al. The values in Table 4 show that 0.94 g Al of the 7 g Al was used in the aluminothermic reduction reactions, Equations (2) and (3). Therefore, the maximum mass of added Al powder remaining to take part in the gas phase reactions is 6.1 g Al. The major species in the calculated gas composition are summarised in Table 7. The calculated loss percentages of Cr, Ni, Cu and Al to the gas phase and the gas phase partial oxygen pressure (P_{O_2}) values are summarised in Table 8.

Table 7. MP10 major gas species concentration (volume%) from the gas-slag-metal powder equilibrium at 2500 °C calculated in FactSage 7.3 thermochemical software (Equilib module) [36].

GramAl	%MgF ₂	%MgF	%Mg	%AlF ₃	%AlF ₂	%AlF	%CaF ₂	%NaF	%Na	%Mn	%CuF	%Cu	%Ni	%SiO	%Cr	%CrF ₃
zero	10	7	9	1	3	5	9	3	4	5	<0.6	17	6	7	6	0.6
3.00	5	5	16	<1	3	12	4	1	3	6	<0.3	17	5	10	9	<0.1
6.10	1	3	20	<0.5	2	18	2	<0.5	3	5	<0.1	16	5	12	10	<0.1

Table 8. MP10 expected metals loss to gas according to gas-slag-metal powder equilibrium at 2500 °C calculated in FactSage 7.3 thermochemical software (Equilib module) [36].

Gram Al	Mass %Cr to Gas	Mass% Ni to Gas	Mass% Cu to Gas	Mass% Al to Gas	P_{O_2} (atm)
zero	13	12	39	0	1.4×10^{-6}
3.00	29	17	65	56	3.1×10^{-7}
6.10	43	21	79	50	9.6×10^{-8}

The calculation results in Tables 7 and 8 indicate that more Cu is vaporised with increased Al added to the gas-slag-metal powder system. Although some CuF is specified as a gas species as displayed in Table 7, the main vaporisation species of copper is metallic copper. Given the similar tendencies of Al and Cu to vaporise, one may expect the replacement of Al gas species originated from Al powder to be substituted by Cu metal powder vaporisation. The calculation results indicate otherwise. A possible reason for this trend is that the vaporisation of copper is reaction controlled and is therefore dependent on the number of reaction sites available at the melt–gas interface [41]. Several surface-active elements such as sulphur and oxygen can fill surface-active sites and limit copper vaporisation. Therefore, the extent of copper vaporisation in the SAW process is less than the calculated gas-slag-metal powder equilibrium quantity. Also, the equilibrium calculation is executed for a set temperature and does not simulate recondensation effects which occur as the gas phase cools.

Improved metal yield from the metal powders to the weld metal was observed after Cu addition to the Al-Ti and Al-Cr metal powders due to the stabiliser effect of copper [25,26]. This effect is less clear in this study due to the combination of Cr with Ni at close to 50% Ni in the Cr-Ni binary alloy system. At this composition point, the alloy liquidus temperature is at its lowest in the Cr-Ni phase diagram at 1342 °C. Based on the insights from the discussion above, our SAW reaction flow diagram is updated to include the chemical behaviour of Cu with Al, Cr and Ni metal powder additions in Figure 8 as shown and discussed below in Section 4.2.

4.2. SAW Reaction Flow Diagram with Al, Cr, Ni and Cu Metal Powder Additions

The SAW reaction flow diagram in Figure 8 is slightly modified from our previous diagram for Al, Cr and Ni metal powder applied in SAW [29]. Flow diagram additions were made as displayed in Figure 8 to account for Cu vaporisation and the stabiliser effect of Cu due to the formation of an initial alloy melt of low liquidus temperature.

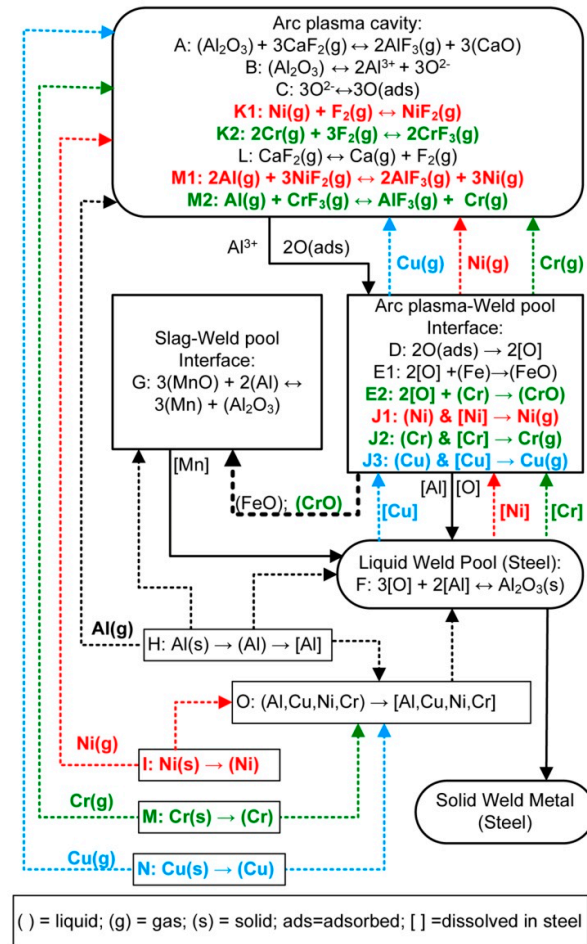


Figure 8. SAW reaction flow diagram with Al, Cr, Ni and Cu powder additions.

Reaction steps A to E are as presented from previous works and represent the transfer of oxygen from the molten flux (slag) to the weld pool [4–6,19,35,42]. Reaction A presents the typical reaction often described in texts on fluoride-based welding fluxes. However, as shown from Gibbs free energy calculations, the formation of Al-fluoride via the reaction $Al(g)$ with $F_2(g)$, Equation (9) in the text, is a more likely reaction for Al-fluoride formation [21,22,28,29]. From experimental evidence presented in previous studies of the SAW process, it was concluded that the molten weld wire droplets from the arc cavity gas phase transfer large excess quantities of oxygen into the weld pool, up to 2000–3000 ppm O [4,5]. This is an important aspect, because once the welding head has moved forward along the welding direction, there is no more arc energy input into the trailing weld pool, and the weld pool subsequently cools to lower temperatures from the high arc plasma temperatures that prevailed underneath the arc, at 2000 to 2500 °C [7,8]. The excess quantity of oxygen stems from the decrease in oxygen solubility in steel with a decrease in weld pool steel temperature. The initial excessive oxygen quantity in the metal droplets is sourced from the dissociation of the less stable oxides in the arc plasma [9]. The metal droplets transfer via the arc plasma–weld pool interface into the weld pool [4,5].

Reaction E1 presents the reaction of the excess oxygen with molten steel at the arc plasma–weld pool interface to form FeO. The trend of increased FeO in the molten flux

(slag) with increased weld metal total ppm O is well established [19,38]. Therefore, the slag FeO content serves as an indicator of the oxygen potential prevailing at the molten flux–weld pool interface [19,38]. The application of Al as a deoxidiser element in our work lowers the oxygen potential prevailing at the molten flux–weld pool interface [21–29]. The result is reduction of MnO according to reaction G in Figure 8. In the same type of reaction, FeO or CrO may also be reduced from the slag. Chromium has a high affinity for oxygen and may therefore easily oxidise to CrO at the arc plasma–weld pool interface; see reaction E2. These aluminothermic reactions, Equations (2)–(5) in Section 3.1 of the text, are exothermic and therefore release chemical energy in the form of heat into the weld pool. This extra added heat is immediately available in the weld pool and can be utilised to melt and dissolve metal powder into the weld pool.

Due to the chemical action of aluminium, the nickel and chromium powders are maintained in the metallic state and melted (reactions I and M) to form the initial alloy pool as a precursor to the dissolution of alloying elements into the weld pool. Since there is an excess of Al added, some of the Al also dissolves directly into the weld pool; see reaction H. The alloy pool, represented as reaction step O, is formed due to the stabiliser effect of Cu in combination with Al by lowering the alloy pool liquidus temperature to form an initial melt into which high-melting-point Cr is melted as identified in our previous works [25,26].

As shown previously, the loss of Cr and Ni in SAW from added metal powders is due to Cr and Ni vaporisation and/or the subsequent reaction of chromium and nickel vapour with fluorine gas to form $\text{CrF}_3(\text{g})$ and $\text{NiF}_2(\text{g})$ [21,28]. Nickel vapour formation at the arc plasma–weld pool interface is presented as reaction J1 in Figure 8, and the reaction of nickel vapour with fluorine gas is presented as reaction K1 in Figure 8. The equivalent reactions for chromium vapour are reactions J2 and K2. These reactions take place in combination with reaction L for the release of $\text{F}_2(\text{g})$ from the dissociation of $\text{CaF}_2(\text{g})$ in the arc cavity. The formation of $\text{F}_2(\text{g})$ in the arc cavity from the dissociation of $\text{CaF}_2(\text{g})$ in the arc plasma of the arc cavity appears possible, since the elements of Ca and F were analysed in the arc cavity gas phase when a CaF_2 -based flux was used in SAW test runs [1,12].

Copper can also be vaporised at the arc plasma–weld pool interface, as indicated in reaction J3. However, from the thermodynamic analyses in Section 4.1 it is clear that copper remains as a metal and does not readily react with fluorine gas. Reactions M1 and M2 in Figure 8 indicate the reaction of aluminium vapour with the chromium and nickel fluorides, $\text{CrF}_3(\text{g})$ and $\text{NiF}_2(\text{g})$, to transform these fluorides to nickel and chromium vapour. In addition to the reaction paths J1 to J3 in which Ni, Cr and Cu are vaporised from the weld pool via the arc plasma–weld pool interface, the direct vaporisation of these elements from the unconstrained metal powders before dissolution into the alloy pool or weld pool is also possible. This reaction path is indicated in Figure 8 by the dotted lines between reactions I, M and N and the arc cavity block.

From the above discussion on gas phase reactions in the presence of added aluminium powder, it is clear that the role of Al in the gas phase reactions is to shift Cr and Ni metal powders to the vapour phase, instead of the oxidation of Cr and Ni metal powders to the slag as CrO, Cr_2O_3 and NiO. The role of Al as presented here is in agreement with our previous similar works on the SAW process in which different metal powder combinations with aluminium were applied [21–29]. The stabiliser role of copper in combination with aluminium is also in agreement with our previous conclusions [24,26].

In summary, the results from this study confirm that copper may be added to Al, Cr and Ni metal powders without changing the oxygen control reactions in SAW. The role of copper is as a stabiliser compound because it lowers the initial alloy melt liquidus temperature to allow high-melting-point metals such as Cr to be melted more efficiently into the weld pool. The gas phase behaviour of copper in the arc cavity is to be vaporised as copper metal and form part of the Al-Si-Mg-Ca-Mn-Fe-Cu-Na-Cr-Ni fluoride phase. However, the vaporisation of copper does not appear to substitute for vapour losses from chromium, nickel and aluminium powders.

5. Conclusions

1. Unconstrained metal powders of Al, Cr Ni and Cu were successfully applied in SAW to alloy carbon steel weld metal, whilst controlling the total weld metal ppm O at an acceptable level.
2. The chemical behaviour of copper metal powder added in SAW is to vaporise as metallic copper and incorporate copper in the Al-Si-Mg-Ca-Mn-Fe-Cu-Na-Cr-Ni fluoride.
3. Copper does not appear to substitute for aluminium in the gas phase, even though both elements have similar vapour pressures at specific temperatures.
4. Copper, in combination with aluminium, has a stabiliser effect in SAW due to its formation of an initial alloy melt of low liquidus temperature, thus decreasing the temperature required to melt high-melting-point metals such as Cr into the weld pool.
5. Nano-strands appear in domes of the 3D slag sample and indicate vaporisation and recondensation of oxy-fluoride.
6. The application of unconstrained metal powders can improve the overall SAW process productivity because it removes the need for the manufacturing of alloyed wire and pre-alloyed powder. Manufacturing of these pre-alloyed wires and powders are expensive, time-consuming steps.

Author Contributions: F.D.B. as inventor conceptualised the work; F.D.B. and T.C. executed the experiments together, interpreted the data together and prepared the manuscript together. All authors have read and agreed to the published version of the manuscript.

Funding: This research was funded in part by the National Research Foundation of South Africa, grant number BRIC171211293679.

Data Availability Statement: The data sets presented in this study are available upon reasonable request to the corresponding author, indicated on the first page.

Conflicts of Interest: The authors declare no conflict of interest. The funders had no role in the design of the study; in the collection, analyses or interpretation of data; in the writing of the manuscript; or in the decision to publish the results.

References

1. Sengupta, V.; Havrylov, D.; Mendez, P.F. Physical phenomena in the weld zone of submerged arc welding—A Review. *Weld. J.* **2019**, *98*, 283–313.
2. O'Brien, A. *Welding Handbook—Materials and Applications, Part 1*, 9th ed.; American Welding Society (AWS): Miami, FL, USA, 2011; Volume 4.
3. Dallam, C.B.; Liu, S.; Olson, D.L. Flux composition dependence of microstructure and toughness of submerged arc HSLA weldments. *Weld. J.* **1985**, *64*, 140–152.
4. Polar, A.; Indacochea, J.E.; Blander, M. Electrochemically generated oxygen contamination in submerged arc welding. *Weld. J.* **1990**, *69*, 68–74.
5. Lau, T.; Weatherly, G.C.; Mc Lean, A. The sources of oxygen and nitrogen contamination in submerged arc welding using CaO-Al₂O₃ based fluxes. *Weld. J.* **1985**, *64*, 343–347.
6. Eagar, T.W. Sources of weld metal oxygen contamination during submerged arc welding. *Weld. J.* **1978**, *57*, 76–80.
7. Chai, C.S.; Eagar, T.W. Slag-metal equilibrium during submerged arc welding. *Metall. Trans. B* **1981**, *12*, 539–547. [[CrossRef](#)]
8. Mitra, U.; Eagar, T.W. Slag-metal reactions during welding: Part I. Evaluation and reassessment of existing theories. *Metall. Trans. B* **1991**, *22*, 65–71. [[CrossRef](#)]
9. Chai, C.S.; Eagar, T.W. Slag metal reactions in binary CaF₂-metal oxide welding fluxes. *Weld. J.* **1982**, *61*, 229–232.
10. Tuliani, S.S.; Boniszewski, T.; Eaton, N.F. Notch toughness of commercial submerged arc weld metal. *Weld. Met. Fabr.* **1969**, *37*, 327–339.
11. Kohno, R.; Takamo, T.; Mori, N.; Nagano, K. New fluxes of improved weld metal toughness for HSLA steels. *Weld. J.* **1982**, *61*, 373–380.
12. Gött, G.; Gericke, A.; Henkel, K.-M.; Uhrlandt, D. Optical and spectroscopic study of a submerged arc welding cavern. *Weld. J.* **2016**, *95*, 491–499.
13. Sengupta, V.; Mendez, P.F. Effect of fluxes on metal transfer and arc length in SAW. *Weld. J.* **2017**, *96*, 334–353.
14. Palm, J.H. How fluxes determine the metallurgical properties of Submerged Arc Welds. *Weld. J.* **1972**, *51*, 358–360.
15. Paniagua-Mercado, A.M.; Lopez-Hirata, V.M.; Saucedo Munoz, M.L. Influence of the chemical composition of flux on the microstructure and tensile properties of submerged-arc welds. *J. Mater. Proc. Technol.* **2005**, *169*, 346–351. [[CrossRef](#)]

16. Bang, K.; Park, C.; Jung, H.; Lee, J. Effects of flux composition on the element transfer and mechanical properties of weld metal in submerged arc welding. *J. Met. Mater. Int.* **2009**, *15*, 471–477. [[CrossRef](#)]
17. Singh, B.; Khan, Z.A.; Siddiquee, A.N. Effect of flux composition on element transfer during Submerged Arc Welding (SAW): A literature review. *Int. J. Curr. Res.* **2013**, *5*, 4181–4186.
18. O'Brien, A. *Welding Handbook—Welding Processes, Part 1*, 9th ed.; American Welding Society (AWS): Miami, FL, USA, 1994; Volume 2.
19. Mitra, U.; Eagar, T.W. Slag metal reactions during submerged arc welding of alloy steels. *Metall. Trans. B* **1984**, *15*, 217–227. [[CrossRef](#)]
20. Hallén, H.; Johansson, K.-E. Use of a Metal Powder for Surface Coating by Submerged Arc Welding. U.S. Patent 6331688 B1, 18 December 2001.
21. Coetsee, T.; De Bruin, F. Aluminium Assisted Nickel Alloying in Submerged Arc Welding of Carbon Steel: Application of Unconstrained Metal Powders. *Appl. Sci.* **2022**, *12*, 5392. [[CrossRef](#)]
22. Coetsee, T.; De Bruin, F. Modification of Flux Oxygen Behaviour via Co-Cr-Al Unconstrained Metal Powder Additions in Submerged Arc Welding: Gas Phase Thermodynamics and 3D Slag SEM Evidence. *Processes* **2022**, *10*, 2452. [[CrossRef](#)]
23. Coetsee, T.; De Bruin, F.J. Improved titanium transfer in Submerged Arc Welding of carbon steel through aluminium addition. *Miner. Process. Extr. Metall. Rev.* **2021**, *43*, 771–774. [[CrossRef](#)]
24. Coetsee, T.; De Bruin, F.J. Reactions at the molten flux-weld pool interface in submerged arc welding. *High Temp. Mater. Processes.* **2021**, *40*, 421–427. [[CrossRef](#)]
25. Coetsee, T.; De Bruin, F. Application of Copper as Stabiliser in Aluminium Assisted Transfer of Titanium in Submerged Arc Welding of Carbon Steel. *Processes* **2021**, *9*, 1763. [[CrossRef](#)]
26. Coetsee, T.; De Bruin, F. Chemical Interaction of Cr-Al-Cu Metal Powders in Aluminum-Assisted Transfer of Chromium in Submerged Arc Welding of Carbon Steel. *Processes* **2022**, *10*, 296. [[CrossRef](#)]
27. Coetsee, T.; De Bruin, F. Aluminium-Assisted Alloying of Carbon Steel in Submerged Arc Welding: Application of Al-Cr-Ti-Cu Unconstrained Metal Powders. *Processes* **2022**, *10*, 452. [[CrossRef](#)]
28. Coetsee, T.; De Bruin, F. Application of Unconstrained Cobalt and Aluminium Metal Powders in the Alloying of Carbon Steel in Submerged Arc Welding: Thermodynamic Analysis of Gas Reactions. *Appl. Sci.* **2022**, *12*, 8472. [[CrossRef](#)]
29. Coetsee, T.; De Bruin, F. Aluminium-Assisted Alloying of Carbon Steel in Submerged Arc Welding with Al-Cr-Ni Unconstrained Metal Powders: Thermodynamic Interpretation of Gas Reactions. *Processes* **2022**, *10*, 2265. [[CrossRef](#)]
30. Raabe, D.; Tasan, C.C.; Springer, H.; Bausch, M. From high-entropy alloys to high-entropy steels. *Steel Res. Int.* **2015**, *86*, 1127–1138. [[CrossRef](#)]
31. Moon, J.; Ha, H.-Y.; Kim, K.-W.; Park, S.-J.; Lee, T.-H.; Kim, S.-D.; Jang, J.H.; Jo, H.-H.; Hong, H.-U.; Lee, B.H.; et al. A new class of lightweight, stainless steels with ultra-high strength and large ductility. *Sci. Rep.* **2020**, *10*, 12140. [[CrossRef](#)]
32. De, S.K.; Srikanth, S.; Saxena, A.K.; Jha, B.K. Copper bearing steels from SAIL and its application. *Int. J. Metall. Eng.* **2016**, *5*, 1–8.
33. Patel, D.; Soman, S.N. Develop a flux cored wire for submerged arc welding of Ni-Mo low alloy steel. *Sadhana* **2020**, *45*, 127. [[CrossRef](#)]
34. Coetsee, T. Phase chemistry of Submerged Arc Welding (SAW) fluoride based slags. *Mater. Res. Technol.* **2020**, *9*, 9766–9776. [[CrossRef](#)]
35. Coetsee, T.; Mostert, R.J.; Pistorius, P.G.H.; Pistorius, P.C. The effect of flux chemistry on element transfer in Submerged Arc Welding: Application of thermochemical modelling. *Mater. Res. Technol.* **2021**, *11*, 2021–2036. [[CrossRef](#)]
36. Bale, C.W.; Bélisle, E.; Chartrand, P.; Deckerov, S.; Eriksson, G.; Gheribi, A.E.; Hack, K.; Jung, I.-H.; Kang, Y.-B.; Melançon, J.; et al. Reprint of: FactSage thermochemical software and databases, 2010–2016. *Calphad* **2016**, *55*, 1–19. [[CrossRef](#)]
37. Coetsee, T.; De Bruin, F. In Situ Modification of CaF₂-SiO₂-Al₂O₃-MgO Flux Applied in the Aluminium-Assisted Transfer of Titanium in the Submerged Arc Welding of Carbon Steel: Process Mineralogy and Thermochemical Analysis. *Minerals* **2022**, *12*, 604. [[CrossRef](#)]
38. Coetsee, T.; De Bruin, F. Insight into the Chemical Behaviour of Chromium in CaF₂-SiO₂-Al₂O₃-MgO Flux Applied in Aluminium-Assisted Alloying of Carbon Steel in Submerged Arc Welding. *Minerals* **2022**, *12*, 1397. [[CrossRef](#)]
39. Kluken, A.O.; Grong, Ø. Mechanisms of inclusion formation in Al-Ti-Si-Mn deoxidized steel weld metals. *Metall. Trans. B* **1989**, *20*, 1335–1349. [[CrossRef](#)]
40. Lau, T.; Weatherly, G.C.; Mc Lean, A. Gas/Metal/Slag reactions in Submerged Arc Welding using CaO-Al₂O₃ based fluxes. *Weld. J.* **1986**, *65*, 31–38.
41. Collur, M.M.; Paul, A.; Debroy, T. Mechanism of alloying element vaporization during laser welding. *Metall. Trans. B* **1987**, *18*, 733–740. [[CrossRef](#)]
42. Mitra, U.; Eagar, T.W. Slag-metal reactions during welding: Part II. Theory. *Metall. Trans. B* **1991**, *22*, 73–81. [[CrossRef](#)]

Disclaimer/Publisher's Note: The statements, opinions and data contained in all publications are solely those of the individual author(s) and contributor(s) and not of MDPI and/or the editor(s). MDPI and/or the editor(s) disclaim responsibility for any injury to people or property resulting from any ideas, methods, instructions or products referred to in the content.